International Journal of Heat and Mass Transfer 170 (2021) 120944

Contents lists available at ScienceDirect

International Journal of Heat and Mass Transfer

journal homepage: www.elsevier.com/locate/hmt

Nanoslot Patterns for Enhanced Thermal Anisotropy of Si Thin Films

Yue Xiao, Qing Hao*

Department of Aerospace and Mechanical Engineering, University of Arizona, Tucson, AZ 85721 USA

ARTICLE INFO

Article history:
Received 30 August 2020
Revised 14 December 2020
Accepted 6 January 2021
Available online 3 February 2021

Keywords:
Offset nanoslots
thermal anisotropy
thin film
thermal management

ABSTRACT

Materials with a large thermal anisotropy can be widely used to guide the heat flow for various energy-related applications. Other than the well-known thermal conductivity contrast along the in-plane and cross-plane directions of a thin film, the in-plane thermal anisotropy within a thin film is less emphasized. However, such a thermal anisotropy can be easily adopted for the thermal management of thin-film-based electronic devices in practice. In this work, two-dimensional Si thin films patterned with through-film nanoslots are studied for their enhanced in-plane thermal anisotropy. Specifically, the anisotropy of the nanoslot pattern can be further increased if rows of nanoslot patterns have an offset. Within the limitation of nanofabrication techniques, offset nanoslot patterns can provide more scopes for tailoring the transport properties. These nanoslot-patterned thin films can be widely used for applications such as heat guide, thermal insulation, and thermoelectrics.

1. Introduction

Within nanostructured materials, the thermal transport can be largely suppressed by the interfacial or boundary scattering of phonons [1]. In addition to the reduced lattice thermal conductivity k_L, the thermal anisotropy can also be critical in certain cases. It is well known that the cross-plane k_L of a film can be lower than the in-plane k_L. Examples can be found for a simple solid film [2], a nanoporous film [3–5], and a superlattice thin film [6]. For thermoelectric (TE) applications, the electrical and thermal properties of a film-like sample must be measured along the same direction to compute the corresponding TE figure of merit (ZT). In naturally formed materials, thermal anisotropy can be found for those with layered atomic structures, e.g., graphite. More recent studies on nanostructured materials also reveal thermal anisotropy for few-layer black phosphorus [7–9], SiC/graphene nanocomposites [10] along the in-plane and cross-plane directions.

Despite these anisotropic thermal conductivities in various structures, it is hard to employ them in real applications. For thin-film-based electronic devices, a large thermal anisotropy for the in-plane heat conduction can be more effective to guide the heat transfer across the chip. Efforts are made by synthesizing in-plane anisotropic materials such as layered TiS_3 [11], black arsenic [12], and black phosphorous nanoribbons [13]. Along another line, a large in-plane thermal anisotropy can be achieved by fabricating anisotropic patterns within a solid film. For example, periodic nanoporous thin films with different cylindrical pore orientation angles are used to tune the in-plane thermal conductivity [14]. Thickness-modulated thin films have also been proposed to modify the in-plane thermal anisotropy [15]. However, such structures require a film to have a relatively large initial thickness to yield contrast by locally reducing the film thickness. When the initial film thickness is already much shorter than majority phonon mean free paths (MFPs), such thickness modification becomes ineffective. In other studies, periodic square pores with different periodic lengths along the x and y directions are patterned on a two-dimensional (2D) thin film to achieve a high thermal anisotropy for the in-plane phonon transport [16].

In this work, a simple but more effective anisotropic pattern is proposed to achieve an even better in-plane k anisotropy within thin films and general 2D materials. In this pattern, periodic nanoslots are arranged with an offset p_0 between two parallel nanoslot rows (Fig. 1a). Such patterns can be found in previous studies on graphene, but the focus is not on thermal anisotropy [17]. In this work, a systematic study utilizing frequency-dependent phonon Monte Carlo (MC) simulations [18,19] is carried out to obtain the thermal conductivities along two major axis directions, which are denoted as k_x and k_y, respectively. It is found that such an offset nanoslot pattern can dramatically suppress k_x while maintaining k_y. As a result, the in-plane thermal anisotropy, which is defined as $\gamma = k_y/k_x$, can be increased from patterns using aligned nanoslots. Other applications using the proposed offset nanoslot patterns, including the TE energy conversion and the heat guide for the thermal management of an electronic device, are also explored in this work.

* Corresponding author.
E-mail address: qinghao@email.arizona.edu (Q. Hao).

https://doi.org/10.1016/j.ijheatmasstransfer.2021.120944
0017-9310/

Nomenclature

2D	Two-dimensional
3D	Three-dimensional
BTE	Boltzmann transport equation
EBL	Electron beam lithography
MC	Monte Carlo
MFP	Mean free path
TE	Thermoelectrics
ZT	Thermoelectric figure of merit

Greek Symbols

Λ_{Bulk}	Bulk phonon mean free path (m)
Λ_{Film}	Effective in-plane phonon mean free path along a solid thin film (m)
α	Phonon suppression function
γ	In-plane thermal conductivity anistropy
σ	Electrical conductivity

Roman Symbols

b	Channel depth of the nanoslot pattern (m)
H_w	Heat-conduction-reduction factor due to porosity
k	Thermal conductivity (W/m•K)
k_L	Lattice thermal conductivity (W/m•K)
k_x	In-plane thermal conductivity along the x direction (W/m•K)
$k_{x,a}$	In-plane thermal conductivity along the x direction with aligned nanoslot patterns (W/m•K)
$k_{x,eff}$	In-plane effective thermal conductivity along the x direction (W/m•K)
$k_{x,o}$	In-plane thermal conductivity along the x direction with offset nanoslot patterns (W/m•K)
k_y	In-plane thermal conductivity along the y direction (W/m•K)
$k_{y,eff}$	In-plane effective thermal conductivity along the y direction (W/m•K)
L_c	Characteristic length of a nanostructure, as determined by the geometry (m)
L_{eff}	Effective characteristic length of a nanostructure (m)
l	Pitch of the nanoslot pattern along the x direction (m)
p	Pitch of the nanoslot pattern along the y direction (m)
p_o	Offset distance of the nanoslot pattern (m)
S	Seebeck coefficient (μV/K)
T	Absolute temperature (K)
w	Neck width between adjacent nanoslots (m)

2. Determining the in-plane thermal anisotropy γ

Frequency-dependent phonon MC simulations are utilized to determine the in-plane thermal anisotropy γ of 2D Si thin films with offset nanoslot patterns. For a 2D thin film, the top and bottom film surfaces are assumed to specularly reflect phonons so that the thermal conductivity is unaffected by the film thickness. By tracking the movement and scattering of individual phonons, the solution for the phonon Boltzmann transport equation (BTE) can be statistically obtained. The exact phonon MFP distribution and complicated three-dimensional structures can be fully considered in these simulations. To improve the computational efficiency, a variance-reduced MC technique developed by Péraud and Hadjiconstantinou is employed [20]. As an input to the phonon MC simulations, fitted bulk phonon MFP Λ_{Bulk} provided by Wang *et al.* is adopted [21]. Only three identical isotropic and sine-shaped acoustic phonon branches are considered. The phonon scattering mechanisms considered include the Umklapp scattering and the impurity scattering [21]. The employed bulk phonon MFPs have been adopted for the phonon MC simulations of nanoporous Si thin films and the predictions can agree well with the experimental data [22,23]. All simulations are performed at 300 K.

Using the boundary condition developed for general periodic structures [24], only one period of the offset nanoslot patterns is selected as the computational domain to simulate k_x and k_y. For each simulation, the sidewalls of the computational domain are enforced to have specular phonon reflection because of the structural symmetry. In Fig. 1b, the nanoslot pattern can be defined using the neck width w between adjacent nanoslots, nanoslot depth b, y-direction pitch p and x-direction pitch l. The offset distance p_o is kept at $p_o = p/2$ (Fig. 1), where the midpoints of the channels and nanoslots are aligned to achieve the maximum suppression of the x-direction thermal transport. As a comparison, the corresponding patterns with aligned nanoslots (i.e., $p_o = 0$) are also simulated for each case. When a 3D thin film with diffusive film-surface phonon scattering is considered, the bulk phonon MFP Λ_{Bulk} can be simply converted into an effective in-plane phonon MFP Λ_{Film} using the Fuchs-Sondheimer model [2]. As a special case, Λ_{Film} is simply equal to Λ_{Bulk} for 2D thin films or atomic thick materials. The rest of the computations is essentially the same [25,26]. The edges of nanoslots are assumed to have completely diffusive phonon scattering. Above 300 K, this assumption is generally valid for rough pore edges introduced by the nanofabrication [22,23,27,28].

3. Results and discussion

3.1. Thermal anisotropy

A systematic study of the thermal anisotropy γ is carried out using the frequency-dependent phonon MC simulations. For lightly doped or undoped Si, the thermal conductivity can be approximately as the lattice part only. Figure 2a shows the x-direction thermal conductivities of 2D Si thin films with offset ($k_{x,o}$) and aligned ($k_{x,a}$) nanoslot patterns, as obtained from frequency-dependent phonon MC simulations. The neck width w of the 2D structures ranges from 20 nm to 120 nm, and Fig. 2a inset illustrates the change of w on the nanoslot geometry. Other adopted dimensions are l=30 nm, p=240 nm, p_o=120 nm, and b=10 nm. Considering the typical 5 nm spatial resolution for electron beam lithography (EBL), the minimum feature size b is controlled at 10 nm to be more realistic. In Fig. 2a, the y-direction lattice thermal conductivity k_y is identical for aligned and offset nanoslot patterns. It is also observed that both $k_{x,o}$ and $k_{x,a}$ increase with an increased w. However, $k_{x,o}$ is insensitive to the dramatic change of the neck width w. Such a trend indicates that the requirement of a small w to suppress the phonon transport can be largely mitigated in offset nanoslot patterns. At the extreme case with w=120 nm, where no overlapping is found between adjacent rows of nanoslots, the $k_{x,o}$ can still be comparable to $k_{x,a}$ with w =20 nm.

With k_x and k_y values, the in-plane thermal anisotropy is calculated (Fig. 2b). For 2D Si thin films with offset nanoslot patterns, $\gamma = k_y/k_x$ for offset nanoslot patterns is consistently higher than that for aligned nanoslot patterns, with the maximum γ=37.5 found. This γ value is significantly larger than the highest $\gamma \approx 12$ for thickness-modulated thin films [15] and the highest $\gamma \approx 18.5$ for nanoporous materials with anisotropic pore lattices [16]. Particularly for phonons with MFPs much longer than the neck width w between nanoslots, the ballistic constriction resistance posed by the neck width can dramatically suppress the contribution of these phonons to the x-direction lattice thermal conductivity [17,29]. Similar discussions for the "ballistic thermal resistance" or Sharvin

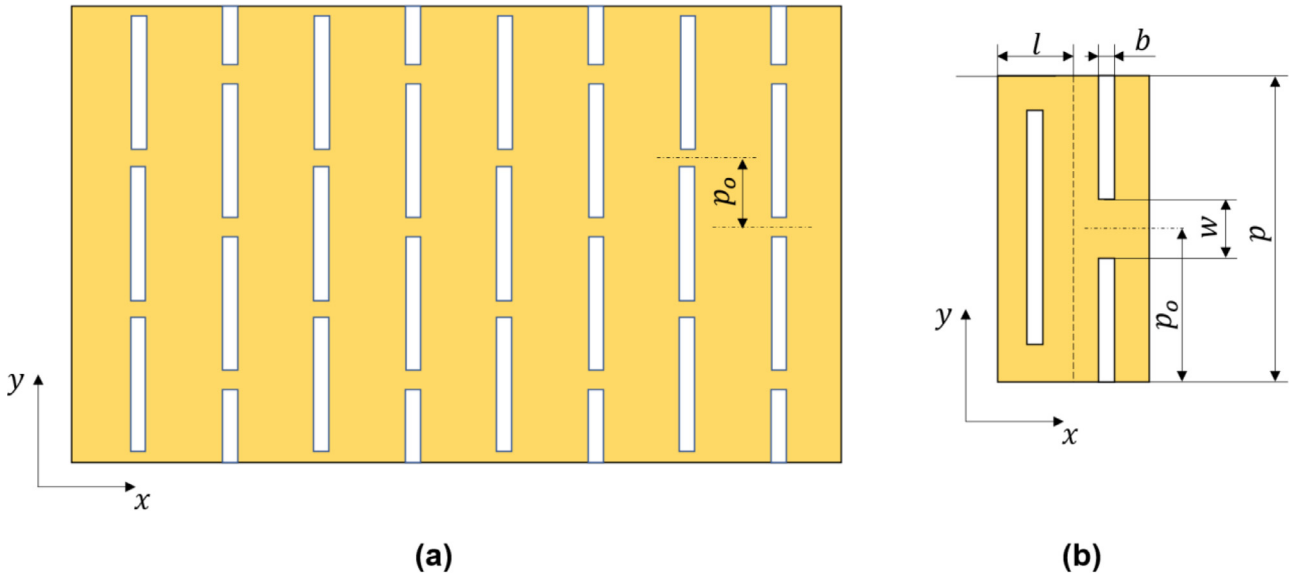

Fig. 1. (a) The offset nanoslot pattern. (b) Illustration of one period of the offset nanoslot pattern, with key geometries and in-plane heat transfer directions marked.

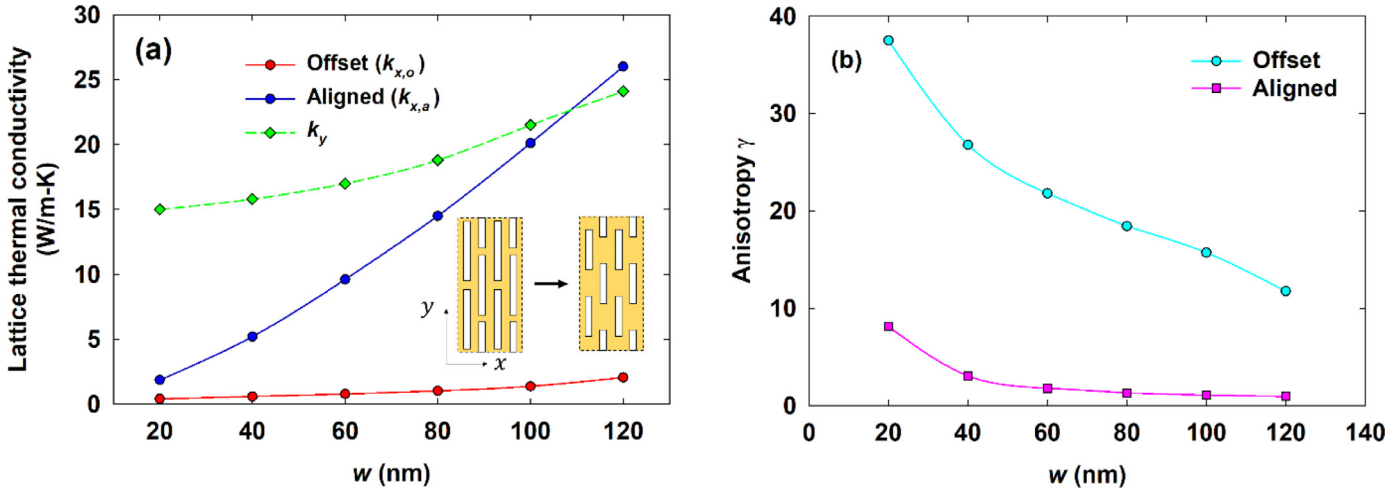

Fig. 2. (a) In-plane lattice thermal conductivities as a function of the neck width w, as predicted by frequency-dependent phonon MC simulations. Inset: Illustration of neck width w change of the offset nanoslot pattern. (b) Comparison of thermal anisotropy γ. Other adopted dimensions are l=30 nm, p=240 nm, p_o=120 nm, and b=10 nm.

resistance [30] can be found in Si nanoribbons with fins attached to the two opposite sides [31], i.e., the fish bone structures [32].

Similar studies are also performed with varied x-direction pitch l. Figure 3a presents the in-plane lattice thermal conductivities with l=30–130 nm, as predicted by frequency-dependent phonon MC simulations. Figure 3a inset illustrates the change of l. Other geometry parameters are w=60 nm, p=240 nm and b=10 nm. With an increasing l and subsequently less cross-sectional reduction on y direction, k_y increases with l. For both offset and aligned nanoslot patterns, k_x will increase because an increased l reduces the suppression of the phonon transport. Such an observation is well reflected in the characteristic length L_c expression developed for the aligned nanoslot patterns [33], nanoladder patterns [34], and fish bone patterns [32]. However, the $k_{x,o}$ is still lower than $k_{x,a}$ for all simulated l values. For a very large l value, both $k_{x,o}$ and $k_{x,a}$ are mainly restricted by the ballistic thermal resistance at the neck width w so that the two values would converge. Figure 3b presents the thermal anisotropy γ. Here 2D Si thin films with offset nanoslot patterns have a maximum thermal anisotropy γ=21.4, comparing with only $\gamma \approx$4.0 with aligned nanoslot patterns. Nanoslot patterns can be optimized to gain a higher thermal anisotropy. In principle, $w/p \ll 1$ and $b/l \ll 1$ are preferred so that k_y can be close to that of a solid film but k_x can be minimized.

For various nanoslot-patterned thin films, a characteristic length L_c can be utilized to modify Λ_{Film} using the Matthiessen's rule [33] to obtain effective in-plane phonon MFP Λ_{eff} of the corresponding nanoslot-patterns:

$$\Lambda_{eff} = \left(\frac{1}{\Lambda_{Film}} + \frac{1}{L_c}\right)^{-1}, \tag{1}$$

and the in-plane thermal conductivity along the x direction, k_x, can be thus determined by

$$k_x = \frac{H_w}{3}\sum_{i=3}\int_{\omega=0}^{\omega_{max,i}} v_{g,i}(\omega)C_i(\omega)\Lambda_{eff,i}(\omega)\, d\omega. \tag{2}$$

In Eq. (2), ω, v_g, and C represent the phonon angular frequency, phonon group velocity and phonon specific heat, respectively. The subscript i stands for the phonon branch, and three acoustic phonon branches are considered in Eq. (2). It is noted that the phonon dispersion may be modified within the narrow neck region that can be viewed as an ultra-fine nanowire. However, the overall impact of this nanowire region on the thermal resistance

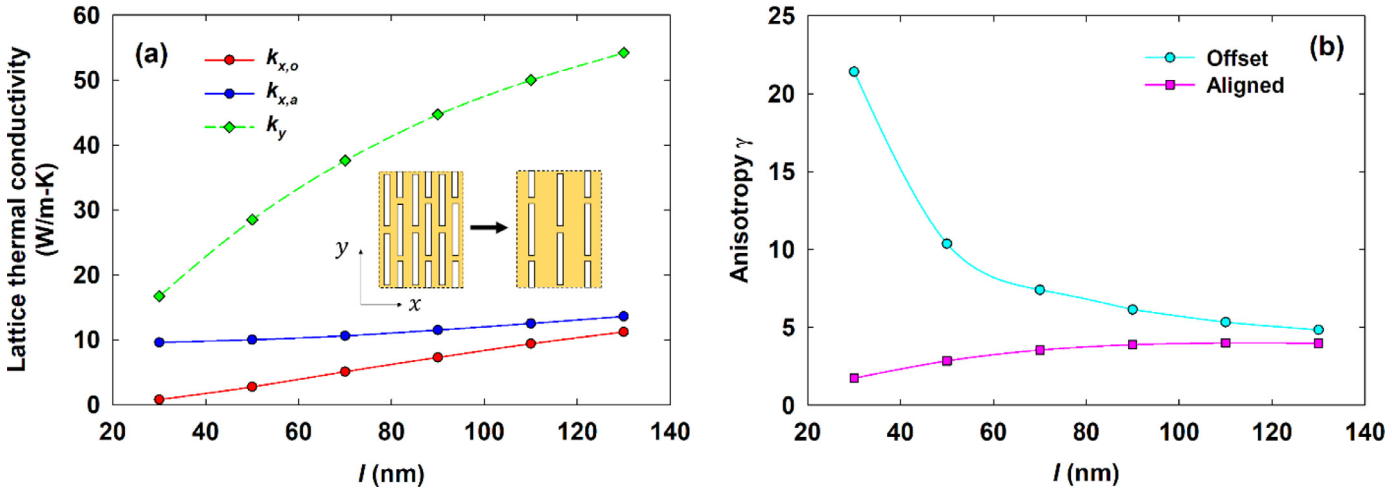

Fig. 3. (a) Different in-plane lattice thermal conductivities predicted by frequency-dependent phonon MC simulations as a function of the x-direction pitch l. Inset: Illustration of pitch l change of the offset nanoslot pattern. (b) Thermal anisotropy γ as a function of l. Other geometry parameters are w=60 nm, p=240 nm and b=10 nm.

of the whole structure can be small when the depth b is very short. Therefore, the bulk phonon dispersion is still assumed for the whole structure for simplification.

For aligned (i.e. no offset) periodic nanoslot patterns with p_o=0 nm and a small channel depth b (Fig. 1b), a simple but accurate analytical model $L_c = 3wl/[4H_w\ (p-w)]$ was previously developed to predict k_x [33]. The correction factor H_w is computed with the Fourier's law as a factor to account for the heat-flow reduction due to decreased cross-sectional area within a porous structure [26,33,35]. For offset nanoslot patterns, it is often observed that with a fixed p, the L_c and subsequently the k_x are decreased with reduced w and l, i.e., weak phonon size effects with increased structure sizes [33]. On the other side, k_y is anticipated to be very close between the offset and aligned nanoslot patterns because the offset shift along the y direction will not remarkably affect the phonon transport along the same y direction.

For a given 2D nanoslot-patterned Si thin film, the characteristic length L_c under a x-direction heat flow can be extracted by matching the simulated in-plane thermal conductivity k_x with predictions based on Eqs. (1) and (2). The extracted L_c can then be used to predict the transport properties of three-dimensional porous thin films with possibly diffusive phonon scattering at the top and bottom film surfaces [19,36]. Figure 4a presents the extracted L_c corresponding to $k_{x,o}$ and $k_{x,a}$ for w=20–120 nm. For offset nanoslot patterns, L_c was maintained at around 13–15 nm regardless of the w value, whereas L_c of aligned nanoslot patterns almost linearly increases with w. A comparison between L_c for aligned and offset nanoslot patterns is also given for increased l (Fig. 4b). Although L_c for offset nanoslot patterns increases at enlarged l values, it is still lower than that for the aligned nanoslot patterns.

The characteristic length L_c also reveals the phonon MFP suppression due to the nanoslot structures with neck width w. A suppression function S can be derived as

$$S(\eta) = \frac{L_c}{\eta w + L_c} H_w, \tag{3}$$

where $\eta = \Lambda_{Film}/w$ [35]. The corresponding S represents the structural suppression of the thermal transport for phonons with a specific in-plane phonon MFP Λ_{Film}. It is observed that when $\eta \to 0$, i.e. $\Lambda_{Film} \ll w$, the suppression function S will converge to the suppression under the Fourier's law, where S=H_w. Equation (3) is verified by performing the frequency-independent phonon MC simulations with a fixed Λ_{Film} that is further varied across the whole phonon MFP spectrum for $S(\eta)$. The top and bottom film surfaces both have specular phonon reflection in these simulations, where possibly diffusive film-surface phonon scattering can be incorporated into $\Lambda_{Film}<\Lambda_{Bulk}$ for a 3D thin film. The results are plotted as symbols in Fig. 4c. A good agreement is observed between Eq. (3) and phonon MC simulations, which further validates the L_c values in Fig. 4a and Eq. (3).

3.2. Anisotropic ZTs along the x and y directions

With a given characteristic length L_c, the corresponding in-plane lattice thermal conductivity can be computed with Eqs. (1) and (2). Because charge carriers have the same boundary scattering as phonons, the same L_c can be used to modify the MFP of charge carriers to compute the electrical properties. The electrical conductivity σ, the Seebeck coefficient S, thermal conductivity k and subsequently the TE figure of merit $ZT = \sigma S^2 T/k$ can be predicted, where T is the absolute temperature. All employed equations and models for the TE property calculations of periodic porous thin films with L_c can be found elsewhere [33,37,38].

An n-type 2D Si thin film with a doping level of 2×10^{20} cm^{-3} is considered. For such heavily doped samples, the impurity-phonon scattering rate, given as $1/\tau_{IM} = A\omega^4$ [39,40], has an increased $A = 1.647 \times 10^{-44}$ s^3 according to studies on heavily doped single-crystal Si films [41]. The neck width is selected as w=5, 20, and 120 nm. Other dimensions are the same as those used in Fig. 2, i.e., l=30 nm, p=240 nm, p_o=120 nm, and b=10 nm. A six-fold degenerate conduction band and a valence band are adopted for Si. The charge carrier scattering by the acoustic phonons and ionized impurities are considered for the employed bulk charge-carrier MFPs. The influence of possible pore-edge charges trapped by surface defects of nanofabricated pores is not considered [38]. In practice, such charge-carrier trapping can deplete nearby charge carriers and build up a potential field to scatter charge carriers.

Figure 5 presents the calculated x-direction ZTs for 2D Si thin films with aligned and offset nanoslot patterns, with w varying from 5 nm to 120 nm. For offset cases, the ZT can still be largely maintained at larger w values for the offset nanoslot patterns due to a L_c value that is insensitive to an increased w value. In comparison, a notable ZT decrease is observed with the increased w for aligned nanoslot patterns. With the same feature sizes for nanofabrication, the calculated ZTs of the offset nanoslot patterns are higher than that of the corresponding aligned nanoslot patterns. For the w=5 nm case, ZT=0.58 is predicted at 1100 K. The results

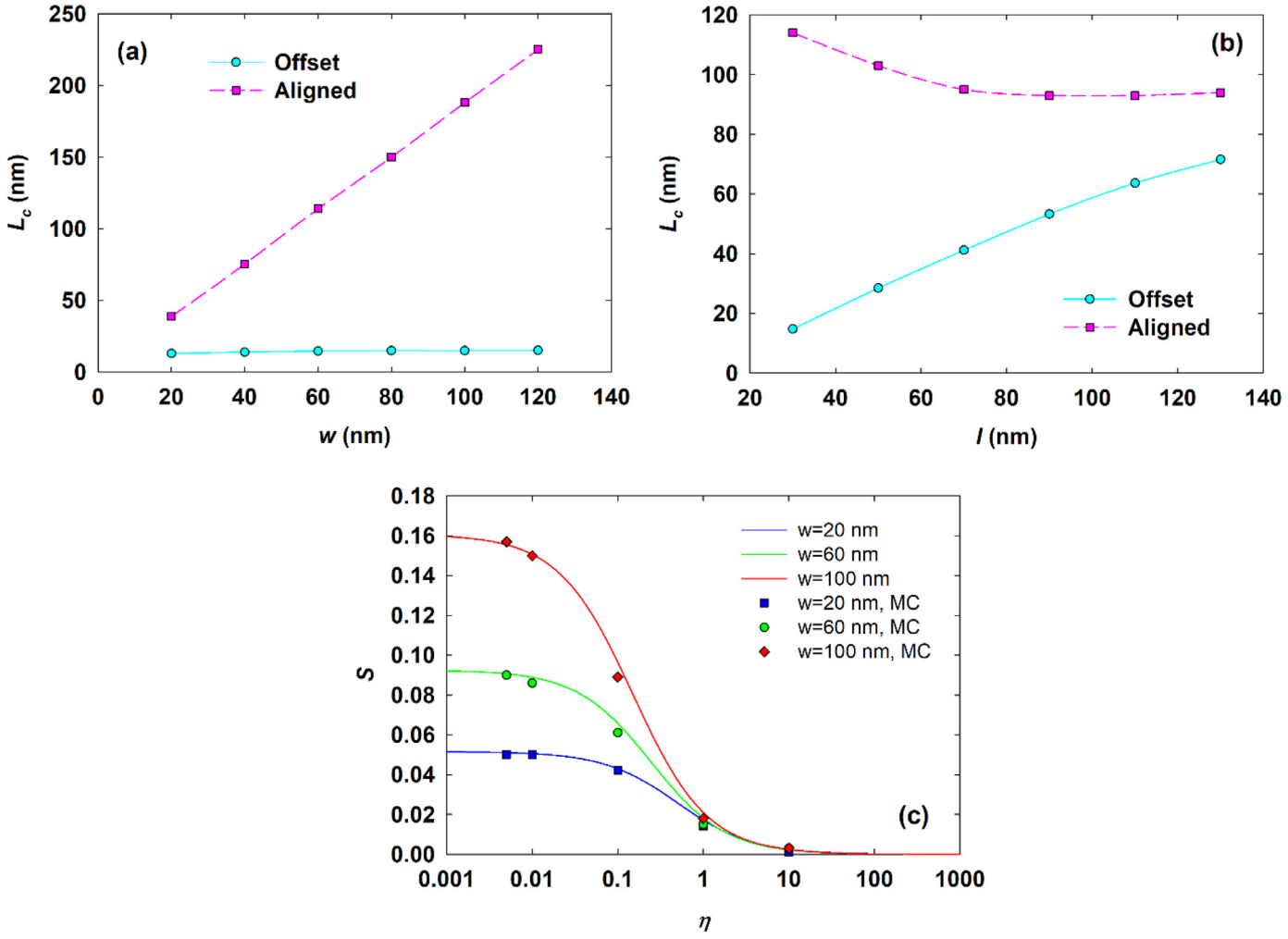

Fig. 4. (a) L_c comparison between offset and aligned nanoslot patterns with respect to the neck width w. Here l=100 nm, p=240 nm and b=10 nm. (b) L_c comparison between offset and aligned nanoslot patterns with respect to the x-direction pitch l. Here w=60 nm, p=240 nm and b=10 nm. (c) Suppression function $S(\eta)$ using Eq. (3), compared to predictions by frequency-independent phonon MC simulations with representative in-plane phonon MFPs (Λ_{Film}) and thus $\eta = \Lambda_{Film}/w$. In (a) and (b), L_c values are extracted from frequency-dependent phonon MC simulations. In (c), S curves are extracted from frequency-independent phonon MC simulations with a varied constant phonon MFP in individual simulations.

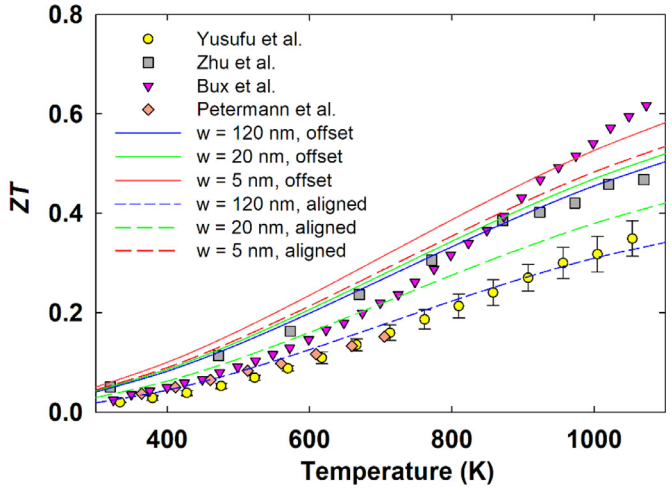

Fig. 5. Temperature-dependent ZTs of nanoslot-patterned 2D Si thin films, in comparison with experimental results of nanostructured bulk Si.

here are further compared with experimental results for nanostructured bulk Si with nanograin boundaries to scattering phonons, including Zhu *et al.* [42], Yusufu *et al.* [43], Petermann *et al.* [44], and Bux *et al.* [45]. For nanoporous Si films, existing thermoelectric measurements are mostly below 300 K and are restricted for thermal conductivities in most studies [26]. Some ZT overestimation may also occur due to measurement errors with nanoporous thin films [46]. In practice, fabricating ultrafine nanoporous patterns across a thin film is also restricted by the aspect ratio of the etching process, where the minimum feature size is smaller than the film thickness by a factor of 3 for dry etching [26]. This limitation can be removed for atomic-thick materials or ultrathin films.

In addition, concerns may exist on the thermal stability of nanoporous Si films for high-temperature applications. In this aspect, one recent study suggests that the possible nanopore contraction can be largely suppressed even at 1173 K for a nanoporous Si thin film placed on a thermally insulated SiO_2 substrate [47]. This can be attributed to the selected substrate that can prevent the spreading of softened Si at elevated temperatures.

3.3. Heat guide

The largely suppressed $k_{x,o}$ but maintained k_y can be widely used to guide heat flow within thin-film-based devices. An early study can be found for thin films patterned with varied circular nanopores [48]. Here Fig. 6a as a film with offset nanoslots

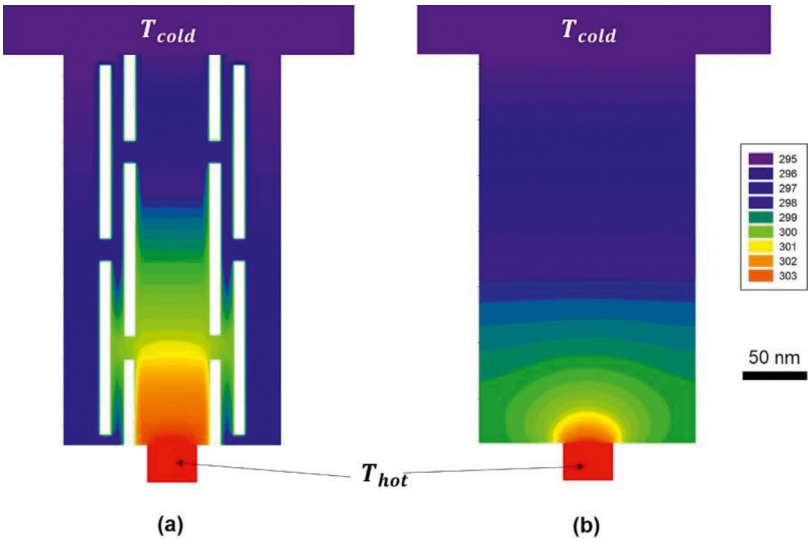

Fig. 6. Temperature profiles for Si thin films (a) with and (b) without the offset nanoslots to guide the heat flow, obtained from frequency-dependent phonon MC simulations.

and Fig. 6b as a comparison solid film demonstrate the use of nanoslot-patterned thin films in guiding the heat flow. Frequency-dependent phonon MC simulations are used to produce Fig. 6. Both three-dimensional films have a thickness of 100 nm, with diffusive phonon scattering on top/bottom film surfaces. The simulated structures are in contact with a heat reservoir with a width of 40 nm at 305 K at the bottom and anther heat reservoir at 295 K at the top. The rest of the sidewalls is adiabatic. Clearly, the heat flow can be largely confined in the middle channel after adding offset nanoslots (Fig. 6a). Without nanoslots, the heat flow spreads within the cross section and becomes one-dimensional when it is close to the cold end (Fig. 6b). Offset nanoslots can also be patterned circularly around a protected region to largely cut off its thermal "talking" to the surrounding, while keeping mechanical connections to the rest of the film. If the structure is well designed, heat can go around the object without leaving a trace to form a "thermal cloak." In a general 2D thin film, the concentric rings as the cloaking region can be carefully designed for their $k(\theta, r)$ in the cylindrical coordinate system [49,50].

4. Conclusion

In summary, periodic nanoslot patterns are explored as an effective way to tune the in-plane thermal anisotropy of a thin film, which can be easily extended to 2D materials such as graphene. Among all simulated cases, the maximum in-plane thermal anisotropy γ can be as high as 37.5 at 300 K, compared with γ=8.1 for aligned nanoslots. The γ value with offset patterns is significantly higher than $\gamma < 19$ for thin films modified with other nanopatterns, including thin films with periodic trenches [15] and rectangular pores [16]. Beyond thermal conductivities, the temperature-dependent ZT is predicted using the extracted characteristic length L_c for both phonons and charge carriers. Comparing with the aligned nanoslot patterns, the same ZT can be achieved in the offset nanoslot patterns with a much larger neck width w to restrict the heat flow. The dramatic suppression of k_x along the direction perpendicular to the neck width can also be used as an effective heat guide, or thermal cloaking within a thin-film device.

Author statement

Qing Hao: Conceptualization, Methodology, Writing of the manuscript; Yue Xiao: Simulation and modeling, Writing- Help to improve some paragraphs.

Declaration of Competing Interest

None.

Acknowledgments

The authors thank the University of Arizona Research computing High Performance Computing (HPC) and High Throughput Computing (HTC) for the allocation of computing time. This work is supported by the National Science Foundation [grant number CBET-1651840] for studies on MC simulations.

References

[1] D.G. Cahill, P.V. Braun, G. Chen, D.R. Clarke, S. Fan, K.E. Goodson, P. Keblinski, W.P. King, G.D. Mahan, A. Majumdar, H.J. Maris, S.R. Phillpot, E. Pop, L. Shi, Nanoscale thermal transport. II. 2003–2012, Applied Physics Reviews 1 (1) (2014) 011305.
[2] G. Chen, Nanoscale Energy Transport and Conversion: A Parallel Treatment of Electrons, Molecules, Phonons, and Photons, Oxford University Press, New York, 2005.
[3] Y.-C. Hua, B.-Y. Cao, Anisotropic Heat Conduction in Two-Dimensional Periodic Silicon Nanoporous Films, The Journal of Physical Chemistry C 121 (9) (2017) 5293–5301.
[4] C. Huang, X. Zhao, K. Regner, R. Yang, Thermal conductivity model for nanoporous thin films, Physica E: Low-dimensional Systems and Nanostructures 97 (2018) 277–281.
[5] Z. Ren, Z. Yu, J.C. Kim, J. Lee, TSV-integrated thermoelectric cooling by holey silicon for hot spot thermal management, Nanotechnology 30 (3) (2018) 035201.
[6] M.N. Luckyanova, J.A. Johnson, A. Maznev, J. Garg, A. Jandl, M.T. Bulsara, E.A. Fitzgerald, K.A. Nelson, G. Chen, Anisotropy of the thermal conductivity in GaAs/AlAs superlattices, Nano letters 13 (9) (2013) 3973–3977.
[7] J. Zhu, H. Park, J.-Y. Chen, X. Gu, H. Zhang, S. Karthikeyan, N. Wendel, S.A. Campbell, M. Dawber, X. Du, M. Li, J.-P. Wang, R. Yang, X. Wang, Revealing the Origins of 3D Anisotropic Thermal Conductivities of Black Phosphorus, Advanced Electronic Materials 2 (5) (2016) 1600040.
[8] B. Smith, B. Vermeersch, J. Carrete, E. Ou, J. Kim, N. Mingo, D. Akinwande, L. Shi, Temperature and Thickness Dependences of the Anisotropic In-Plane Thermal Conductivity of Black Phosphorus, Advanced Materials 29 (5) (2017) 1603756.
[9] Z. Luo, J. Maassen, Y. Deng, Y. Du, R.P. Garrelts, M.S. Lundstrom, P.D. Ye, X. Xu, Anisotropic in-plane thermal conductivity observed in few-layer black phosphorus, Nature Communications 6 (2015) 8572.
[10] C. Chen, X. Han, H. Shen, Y. Tan, H. Zhang, Y. Qin, S. Peng, Preferentially oriented SiC/graphene composites for enhanced mechanical and thermal properties, Ceramics International (2020).
[11] H. Liu, X. Yu, K. Wu, Y. Gao, S. Tongay, A. Javey, L. Chen, J. Hong, J. Wu, Extreme in-plane thermal conductivity anisotropy in titanium trisulfide caused by heat-carrying optical phonons, Nano Letters 20 (7) (2020) 5221–5227.
[12] Y. Chen, C. Chen, R. Kealhofer, H. Liu, Z. Yuan, L. Jiang, J. Suh, J. Park, C. Ko, H.S. Choe, J. Avila, M. Zhong, Z. Wei, J. Li, S. Li, H. Gao, Y. Liu, J. Analytis, Q. Xia,

M.C. Asensio, J. Wu, Black Arsenic: A Layered Semiconductor with Extreme In-Plane Anisotropy, Advanced Materials 30 (30) (2018) 1800754.
[13] S. Lee, F. Yang, J. Suh, S. Yang, Y. Lee, G. Li, H.Sung Choe, A. Suslu, Y. Chen, C. Ko, J. Park, K. Liu, J. Li, K. Hippalgaonkar, J.J. Urban, S. Tongay, J. Wu, Anisotropic in-plane thermal conductivity of black phosphorus nanoribbons at temperatures higher than 100 K, Nature Communications 6 (1) (2015) 8573.
[14] S. Didenko, T. M'Bah, A. Massoud, V. Lacatena, M. Haras, R. Orobtchouk, J.-M. Bluet, P.-O. Chapuis, E. Dubois, J.-F. Robillard, Artificially-induced anisotropic heat flow in 2D patterned membranes, Eurotherm 111: Nanoscale and Microscale Heat Transfer VI, 2018.
[15] Y. Zeng, A. Marconnet, Tuning the Anisotropy of In-Plane Thermal Conduction in Thin Films by Modulating Thickness, Physical Review Applied 9 (1) (2018) 011001.
[16] G. Romano, A.M. Kolpak, Thermal anisotropy enhanced by phonon size effects in nanoporous materials, Applied Physics Letters 110 (9) (2017) 093104.
[17] B.-Y. Cao, W.-J. Yao, Z.-Q. Ye, Networked nanoconstrictions: An effective route to tuning the thermal transport properties of graphene, Carbon 96 (2016) 711–719.
[18] Q. Hao, G. Chen, M.-S. Jeng, Frequency-dependent Monte Carlo simulations of phonon transport in two-dimensional porous silicon with aligned pores, Journal of Applied Physics 106 (11) (2009) 114321.
[19] Q. Hao, Y. Xiao, H. Zhao, Characteristic length of phonon transport within periodic nanoporous thin films and two-dimensional materials, Journal of Applied Physics 120 (6) (2016) 065101.
[20] J.-P.M. Péraud, N.G. Hadjiconstantinou, Efficient simulation of multidimensional phonon transport using energy-based variance-reduced Monte Carlo formulations, Physical Review B 84 (20) (2011) 205331.
[21] Z. Wang, J.E. Alaniz, W. Jang, J.E. Garay, C. Dames, Thermal Conductivity of Nanocrystalline Silicon: Importance of Grain Size and Frequency-Dependent Mean Free Paths, Nano Letters 11 (6) (2011) 2206–2213.
[22] Q. Hao, D. Xu, H. Zhao, Y. Xiao, F.J. Medina, Thermal Studies of Nanoporous Si Films with Pitches on the Order of 100 nm—Comparison between Different Pore-Drilling Techniques, Scientific reports 8 (1) (2018) 9056.
[23] Y. Xiao, D. Xu, F.J. Medina, S. Wang, Q. Hao, Thermal Studies of Nanoporous Thin Films with Added Periodic Nanopores — A New Approach to Evaluate the Importance of Phononic Effects, Materials Today Physics (2020) 100179.
[24] Q. Hao, G. Chen, M.-S. Jeng, Frequency-dependent Monte Carlo simulations of phonon transport in two-dimensional porous silicon with aligned pores, Journal of Applied Physics 106 (11) (2009) 114321–114330.
[25] Q. Hao, Y. Xiao, S. Wang, Two-step modification of phonon mean free paths for thermal conductivity predictions of thin-film-based nanostructures, International Journal of Heat and Mass Transfer 153 (2020) 119636.
[26] Y. Xiao, Q. Chen, D. Ma, N. Yang, Q. Hao, Phonon Transport within Periodic Porous Structures — From Classical Phonon Size Effects to Wave Effects, ES Materials & Manufacturing 5 (2019) 17.
[27] N.K. Ravichandran, A.J. Minnich, Coherent and incoherent thermal transport in nanomeshes, Physical Review B 89 (20) (2014) 205432.
[28] A. Jain, Y.-J. Yu, A.J. McGaughey, Phonon transport in periodic silicon nanoporous films with feature sizes greater than 100 nm, Physical Review B 87 (19) (2013) 195301.
[29] R. Prasher, Predicting the Thermal Resistance of Nanosized Constrictions, Nano Letters 5 (11) (2005) 2155–2159.
[30] Y. Sharvin, On the possible method for studying fermi surfaces, Sov. Phys. JETP 21 (1965) 655.
[31] L. Yang, Y. Zhao, Q. Zhang, J. Yang, D. Li, Thermal transport through fishbone silicon nanoribbons: unraveling the role of Sharvin resistance, Nanoscale 11 (17) (2019) 8196–8203.
[32] J. Maire, R. Anufriev, T. Hori, J. Shiomi, S. Volz, M. Nomura, Thermal conductivity reduction in silicon fishbone nanowires, Scientific Reports 8 (1) (2018) 4452.
[33] Q. Hao, Y. Xiao, Periodic Nanoslot Patterns as an Effective Approach to Improving the Thermoelectric Performance of Thin Films, Physical Review Applied 13 (6) (2020) 064020.
[34] W. Park, J. Sohn, G. Romano, T. Kodama, A. Sood, J.S. Katz, B.S.Y. Kim, H. So, E.C. Ahn, M. Asheghi, A.M. Kolpak, K.E. Goodson, Impact of thermally dead volume on phonon conduction along silicon nanoladders, Nanoscale 10 (23) (2018) 11117–11122.
[35] Q. Hao, Y. Xiao, Q. Chen, Determining phonon mean free path spectrum by ballistic phonon resistance within a nanoslot-patterned thin film, Materials Today Physics 10 (2019) 100126.
[36] Q. Hao, Y. Xiao, H. Zhao, Analytical model for phonon transport analysis of periodic bulk nanoporous structures, Applied Thermal Engineering 111 (2017) 1409–1416.
[37] Q. Hao, H. Zhao, D. Xu, Thermoelectric studies of nanoporous thin films with adjusted pore-edge charges, Journal of Applied Physics 121 (9) (2017) 094308.
[38] Q. Hao, Y. Xiao, Electron Monte Carlo simulations of nanoporous Si thin films—The influence of pore-edge charges, Journal of Applied Physics 125 (6) (2019) 064301.
[39] P.G. Klemens, The Scattering of Low-Frequency Lattice Waves by Static Imperfections, Proceedings of the Physical Society. Section A 68 (12) (1955) 1113–1128.
[40] J.M. Ziman, XVII. The effect of free electrons on lattice conduction, The Philosophical Magazine: A Journal of Theoretical Experimental and Applied Physics 1 (2) (1956) 191–198.
[41] M. Asheghi, K. Kurabayashi, R. Kasnavi, K.E. Goodson, Thermal conduction in doped single-crystal silicon films, Journal of Applied Physics 91 (8) (2002) 5079–5088.
[42] G.H. Zhu, H. Lee, Y.C. Lan, X.W. Wang, G. Joshi, D.Z. Wang, J. Yang, D. Vashaee, H. Guilbert, A. Pillitteri, M.S. Dresselhaus, G. Chen, Z.F. Ren, Increased Phonon Scattering by Nanograins and Point Defects in Nanostructured Silicon with a Low Concentration of Germanium, Physical Review Letters 102 (19) (2009) 196803.
[43] A. Yusufu, K. Kurosaki, Y. Miyazaki, M. Ishimaru, A. Kosuga, Y. Ohishi, H. Muta, S. Yamanaka, Bottom-up nanostructured bulk silicon: a practical high-efficiency thermoelectric material, Nanoscale 6 (22) (2014) 13921–13927.
[44] N. Petermann, N. Stein, G. Schierning, R. Theissmann, B. Stoib, M.S. Brandt, C. Hecht, C. Schulz, H. Wiggers, Plasma synthesis of nanostructures for improved thermoelectric properties, Journal of Physics D: Applied Physics 44 (17) (2011) 174034.
[45] S.K. Bux, R.G. Blair, P.K. Gogna, H. Lee, G. Chen, M.S. Dresselhaus, R.B. Kaner, J.-P. Fleurial, Nanostructured Bulk Silicon as an Effective Thermoelectric Material, Advanced Functional Materials 19 (15) (2009) 2445–2452.
[46] J. Lim, H.-T. Wang, J. Tang, S.C. Andrews, H. So, J. Lee, D.H. Lee, T.P. Russell, P. Yang, Simultaneous Thermoelectric Property Measurement and Incoherent Phonon Transport in Holey Silicon, ACS Nano 10 (1) (2016) 124–132.
[47] Q. Hao, Y. Xiao, F. Medina, Annealing Studies of Nanoporous Si Thin Films Fabricated by Dry Etch, ES Materials & Manufacturing (2019).
[48] R. Anufriev, A. Ramiere, J. Maire, M. Nomura, Heat guiding and focusing using ballistic phonon transport in phononic nanostructures, Nature Communications 8 (2017) 15505.
[49] Y. Zhang, H. Xu, B. Zhang, Design, implementation, and extension of thermal invisibility cloaks, AIP Advances 5 (5) (2015) 053402.
[50] T. Han, T. Yuan, B. Li, C.-W. Qiu, Homogeneous Thermal Cloak with Constant Conductivity and Tunable Heat Localization, Scientific Reports 3 (1) (2013) 1593.